

Fast tailward flows in the plasma sheet boundary layer during a substorm on 9 March 2008: THEMIS observations

A. M. Du,¹ R. Nakamura,² T. L. Zhang,² E. V. Panov,² W. Baumjohann,² H. Luo,¹ W. Y. Xu,¹ Q. M. Lu,³ M. Volwerk,² A. Retinò,² B. Zieger,² V. Angelopoulos,⁴ K.-H. Glassmeier,⁵ J. P. McFadden,⁶ and D. Larson⁶

Received 25 July 2010; revised 8 December 2010; accepted 27 December 2010; published 23 March 2011.

[1] Tailward flows in the plasma sheet boundary layer (PSBL) were observed simultaneously by the five Time History of Events and Macroscale Interactions during Substorms (THEMIS) probes at down-tail distances $X \sim 7.6$ to $\sim 17.6 R_E$ for ~ 10 min during an interval of successive substorm intensification in a storm time on 9 March 2008. The flows first occurred close to Earth and then propagated along the magnetic field lines in the PSBL with a speed of ~ 150 – 350 km s^{-1} . We show that the occurrence of tailward flows is highly dependent on proximity to the plasma sheet boundary. Higher speeds occurred in the outer part of the PSBL, while either lower tailward speeds (or even earthward flows) were seen in the inner part of the PSBL. The tailward flow occurrence increased during magnetotail stretching and decreased or ceased during magnetic field dipolarizations. These PSBL tailward flows near the Earth can be understood as an outflow of the earthward flows that essentially empty the central plasma sheet. The tailward flows along the field line filled the void left behind by the dipolarization front.

Citation: Du, A. M., et al. (2011), Fast tailward flows in the plasma sheet boundary layer during a substorm on 9 March 2008: THEMIS observations, *J. Geophys. Res.*, 116, A03216, doi:10.1029/2010JA015969.

1. Introduction

[2] The energy carried by the solar wind is initially converted to electromagnetic energy (and can be viewed as to be stored in the magnetic field, primarily in the magnetotail) [Kamide et al., 1998]. The energy of a storm/substorm could be supplied from delayed release of the energy stored in the magnetotail [Tsurutani and Gonzalez, 1995; Du et al., 2008]. Bursty Bulk Flows (BBFs) account for 70–100% of the total earthward transport of plasma, energy, and magnetic flux in the midtail plasma sheet [Angelopoulos et al., 1994]. During a storm, the configuration of the magnetotail becomes very complex. The neutral X line is occasionally formed close to Earth during magnetospheric storms, and the ring current can affect the plasma sheet dynamics [Ohtani and Mukai,

2008]. Following the BBFs, the plasma sheet boundary expands outward and newly closed plasma sheet flux tubes are formed and filled by plasma in an impulsive reconnection process [Sergeev et al., 1996; Nakamura et al., 2004; Wang et al., 2008]. The formation of new auroral arcs is accompanied by the equatorward plasma convection associated with the reconnection.

[3] The plasma sheet boundary layer (PSBL) is an active region between the lobe and central plasma sheet [Frank, 1976; Eastman et al., 1984]. Baumjohann et al. [1988] reported average ion moments in the PSBL, and found that the PSBL is not a transition region but is indeed a unique layer where crucial parameters like ion density and plasma- β remain on nearly constant levels. Typical values in the PSBL for ion density and β are ~ 0.1 – 0.5 cm^{-3} and ~ 0.01 – 0.5 , respectively. The PSBL is distinguished from the lobe as a region where keV electrons and keV ions are measured, yet at much lower densities and pressures than in the plasma sheet closer to the neutral sheet. High-speed flows occur in the PSBL, quite often under all levels of magnetic activity [Baumjohann et al., 1988] though occasional exceptions have been reported [Angelopoulos et al., 1993]. Most of these high-speed flows are field-aligned, and are directed toward the Earth and last for less than 2 min.

[4] Flows in the PSBL are typically a superposition of one or more beams on a cold (mantle-like) population, with the most intense beams occurring at higher energies often during substorm recovery [Lui et al., 1983]. They typically consist of unidirectional or counterstreaming ion beams.

¹Institute of Geology and Geophysics, Chinese Academy of Sciences, Beijing, China.

²Space Research Institute, Austrian Academy of Sciences, Graz, Austria.

³CAS Key Laboratory of Basic Plasma Physics, School of Earth and Space Sciences, University of Science and Technology of China, Hefei, China.

⁴Institute of Geophysics and Planetary Physics, University of California, Los Angeles, California, USA.

⁵Institut für Geophysik und extraterrestrische Physik, Technische Universität Braunschweig, Brunswick, Germany.

⁶Space Science Laboratory, University of California, Berkeley, California, USA.

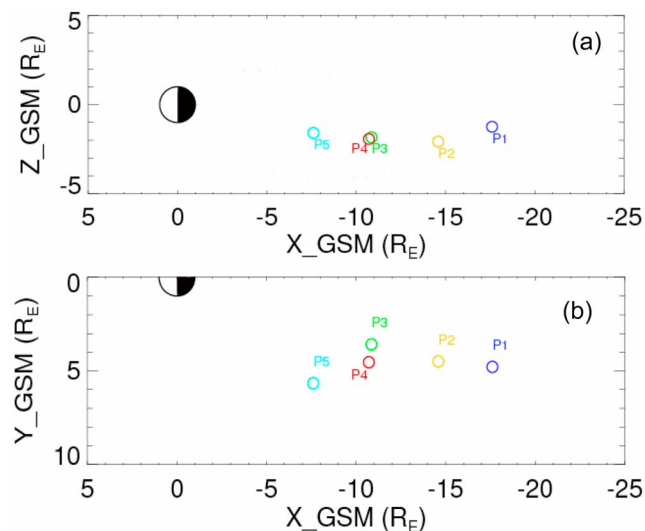


Figure 1. Locations of the five probes of THEMIS in (a) the X - Z plane and (b) the X - Y plane in GSM coordinates at 0718 UT on 9 March 2008.

Earthward directed ion beams are often observed close to the lobes, while counterstreaming beams are observed further away from the lobes, deeper within the plasma sheet [Takahashi and Hones, 1988; Nakamura *et al.*, 1992]. Eastman *et al.* [1984] demonstrated that the main feature in the ion velocity distributions in the PSBL is the earthward flowing ion beams and their counterpart, an antisunward flowing ion beams at high energy. The ion velocity distributions were shown to evolve from one earthward flowing ion beam to a counterstreaming distribution and then on to a more isotropic distribution [Lennartsson *et al.*, 2009]. Williams [1981] suggested counterstreaming ion distributions as the result from near-Earth mirroring of ion beams. Cowley *et al.* [1984] identified unidirectional energetic ions in the distant tail PSBL and suggested that the ion beams are the result of a reconnection process. In the midtail ($X_{GSE} \sim -20 R_E$), Hones *et al.* [1982] and Eastman *et al.* [1984] interpreted a net tailward flow in the PSBL (observed by ISEE 1 and 2) two minutes after a net earthward flow as the tailward movement of a plasmoid that formed at the tailward side of a neutral line.

[5] Recently, 3-D MHD simulations by Birn *et al.* [2004] showed an additional generation mechanism and new propagation features of tailward flows in the PSBL. They found that tailward flows develop in the PSBL when earthward flows from a low-density dipolarized flow burst (a.k.a. bubble) are observed closer to the Earth. In their model, the speed of the tailward flow increases when the earthward flow interacts with the inner edge of the plasma sheet and starts being reduced. The tailward flow fills the plasma void left behind by the earthward moving bubble. Panov *et al.* [2010a, 2010b] found that the tailward flows can result from the bouncing of earthward flows at the strong field and high-pressure plasma region near the inner edge of the plasma sheet. An important finding of Ashour-Abdalla *et al.* [2002, 2009] was that the earthward flow from a tail neutral line reversed direction in the inner magnetosphere and

formed a large-scale vortical nightside convection pattern. The flow reversal and formation of the tail vortices may be the result of the simulation's earthward convection being limited by high near-Earth plasma pressure and/or by line tying caused by the high ionospheric conductance. Furthermore, in Birn *et al.*'s [2004] simulation, the tailward flows in the PSBL are dependent on the balance between plasma and magnetic pressure. In low- β regions like the PSBL, the pressure balance along the field line is restored by the magnetic pressure. As a consequence, the plasma pressure is no longer constant along a flux tube and flows will take place out of the central plasma sheet (CPS) into the PSBL [Birn *et al.*, 2004].

[6] In this paper we present the spatial distribution of prolonged tailward flows in the PSBL using Time History of Events and Macroscale Interactions during Substorms (THEMIS) observations. We attempt to clarify the role of the tailward PSBL flows in the mass and energy transport of the Earth's magnetotail.

2. Data Analysis

[7] Data from the five THEMIS probes are used to study variations of the magnetic field and plasma flows in the magnetotail [Angelopoulos, 2008; Sibeck and Angelopoulos, 2008]. The 3 s (spin period) resolution magnetic field data are from the THEMIS fluxgate magnetometers (FGM) [Auster *et al.*, 2008]. The 3 s resolution particle data are from the THEMIS Electrostatic Analyzers (ESA) [McFadden *et al.*, 2008]. Figure 1 shows the locations of the five probes of THEMIS (P1, through P5) in the GSM X - Z plane (Figure 1a) and the X - Y plane (Figure 1b) at 0718 UT on 9 March 2008. The probes were aligned along X_{GSM} between 7.6 and 17.6 R_E , with a spread in Y_{GSM} from 3.6 to 5.6 R_E , and in Z_{GSM} from -1.2 to $-2.1 R_E$. P5 was the most earthward satellite while P1 was most tailward. P3 was most duskward and P5 was most dawnward. The most northward satellite was P4.

[8] Figure 2 shows the X component of the ion velocity, V_x , for the five THEMIS probes. It is interesting to note that the tailward flow was observed at all of the five probes during the interval of 1715 ~ 1725 UT. The average duration of the tailward flow is about 5 ~ 10 min; however, the start time, the duration, and the flow speed are different for each probe. Parameters of the tailward flow such as duration, maximum flow velocity, plasma- β , ion density, plasma pressure and magnetic pressure are listed in Table 1. In order to eliminate the effects of outliers, we use median instead of mean for plasma- β , ion density, plasma pressure and magnetic pressure.

[9] In Figure 3, the first through ninth panels are interplanetary ACE (black line) and Cluster C1 (blue line) data during 8–9 March 2008. The instruments and the spacecraft of ACE are described by Stone *et al.* [1998]. The ACE data were obtained from OMNI database. They were spacecraft-specific, 1 min averaged, field/plasma ACE data sets shifted to the bow shock nose using a combination of minimum variance and cross product phase front normal determination techniques. Cluster C1 [Balogh *et al.*, 2001] was located in front of the bow shock during the interval of 0100 ~ 0900 UT on 9 March 2008. Its GSM coordinates were (19.2, -1.1 , -8.1) R_E . Figure 3 shows, from top to bottom, the plasma

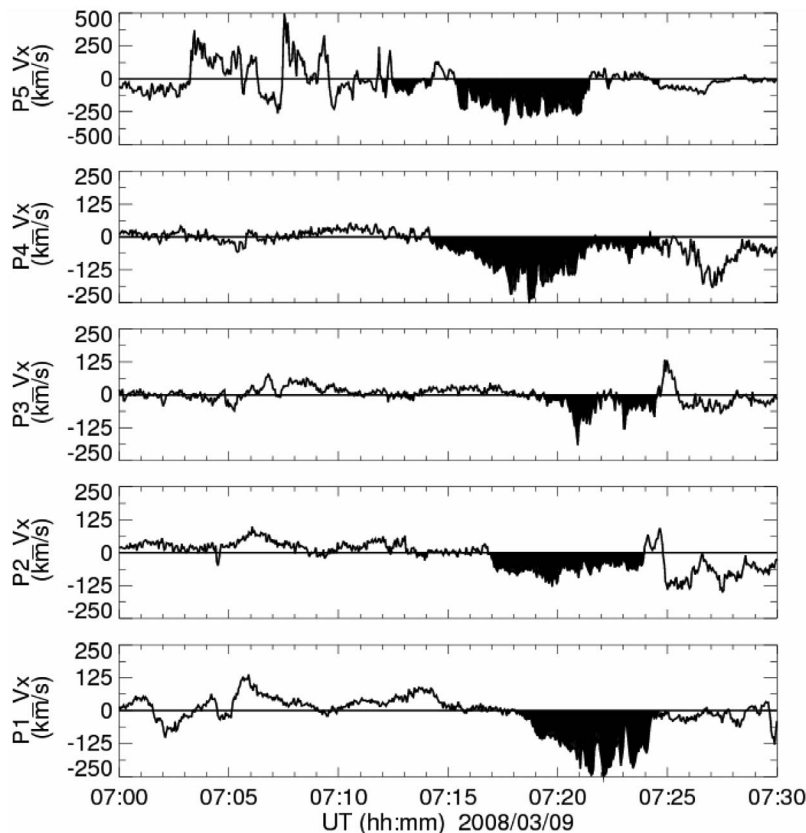


Figure 2. The X component of the ion velocity, V_x , for five probes of THEMIS from P5 to P1 on 9 March 2008.

temperature, T_p , the solar wind velocity, V_{sw} , the proton number density, N_p , the solar wind dynamic pressure, P_{dyn} , interplanetary magnetic field (IMF) components B_x , B_y , and B_z , and magnitude, B_T , and the interplanetary electric field, E_y . In Figure 3, the data from the Cluster satellite were not shifted to take into account solar wind convection delays between the Cluster satellite and magnetosphere. Cluster C1 is located just in front of bow shock. In general, the large-scale features of the IMF components observed by ACE at L1 are quite similar to those observed by Cluster C1 during the interval of 0100 ~ 0900 UT on 9 March 2008. We considered the IMF features used are indeed those that impinged upon the magnetosphere during the storm/substorm.

[10] The tenth and eleventh panels of Figure 3 display the 1 min resolution AE and $SYM-H$ indices. The 1 min resolution $SYM-H$ index, which is essentially the same as the hourly Dst index [Sugiura and Poros, 1971] except in terms

of the time resolution, does not show any statistically significant development after the onset of substorms [Iyemori and Rao, 1996]. We used the $SYM-H$ index only because of its high time resolution.

[11] During the period of 8–9 March 2008, the $SYM-H$ showed a minimum of -100 nT, indicating that the event we are discussing in this paper was happening during a storm time (see Figure 3). From the IMF data we conclude that this storm was associated with a corotating interaction region (CIR) on the basis of its association with a region of compressed plasma, indicated by enhanced plasma densities (~ 40 cm^{-3}) and magnetic field intensities (~ 20 nT), lying at the leading edge of a high-speed stream. The CIR was also identified by Mason *et al.* [2009]. It is noted that the solar wind speed increases from ~ 350 km s^{-1} to ~ 650 km s^{-1} through the storm. The unusually high densities are probably associated with the heliospheric plasma sheet encompassing the heliospheric current sheet that was crossed at

Table 1. Parameters of Duration of Flows, the Maximum of Flow Velocity, and the Median of Plasma Beta, Ion Density, Plasma Pressure, and Magnetic Pressure During the Tailward Flow Interval for Five Probes of THEMIS

Satellites	Location [X, Y, Z] (R_E)	Duration (UT)	V_x Max (km s^{-1})	Beta	Density (cm^{-3})	P_{thermal} (nPa)	P_{mag} (nPa)
P5 (THA)	[-7.6, 5.6, -1.6]	0715:30 ~ 0721:30	-347	0.010	0.117	0.027	2.93
P4 (THE)	[-10.7, 4.5, -1.9]	0714:30 ~ 0721:30	-250	0.017	0.148	0.031	1.66
P3 (THD)	[-10.9, 3.6, -1.8]	0719:20 ~ 0724:40	-191	0.023	0.141	0.035	1.57
P2 (THC)	[-14.6, 4.5, -2.1]	0717:00 ~ 0724:00	-128	0.068	0.219	0.068	1.07
P1 (THB)	[-17.6, 4.8, -1.2]	0718:05 ~ 0725:39	-244	0.78	0.318	0.192	0.27

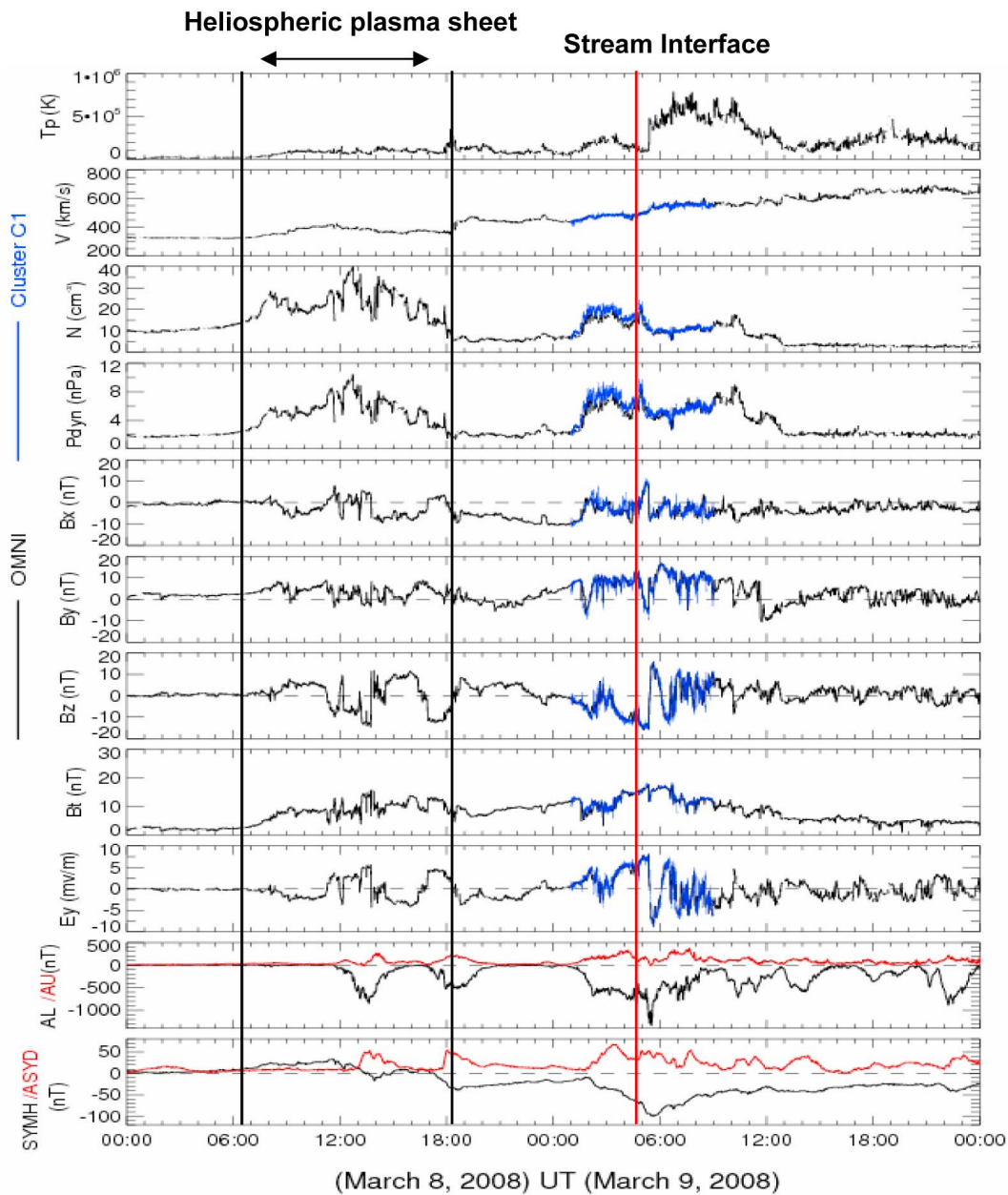


Figure 3. Interplanetary ACE (black line) and Cluster C1 (blue line) data and the geomagnetic index AL/AU and $SYM-H/ASYD$ during 8–9 March 2008. The heliospheric plasma sheet is marked by two black vertical lines, and the red vertical line indicates the stream interface.

~1200 UT on 9 March 2008. There are two increases of the ion density at ~0700 UT of 8 March and ~0100 UT of 9 March, respectively. When the heliospheric plasma sheet (indicated by two vertical black lines shown in Figure 3) swept over the Earth the $SYM-H$ index decreased to ~-50 nT, and recovered after the density increase passed by. Two southward turnings of IMF Bz during this interval caused two isolated substorms at ~1200 UT and ~1700 UT on 8 March 2008. For the second increase of the ion density at ~0100 UT of 9 March, IMF Bz turned southward. $SYM-H$ began to decrease and arrived at a minimum (~-100 nT) at ~0520 UT. The AL index sharply decreased to ~-500 nT in 30 min after ~0130 UT.

[12] The Stream Interface, a narrow structure (often a discontinuity) separating accelerated slow solar wind and decelerated fast stream plasma, is a prominent feature of CIRs. The interface (marked by the vertical red line) is indicated by a relatively abrupt jump in plasma density, and increasing V_{sw} and T_p . The T_p was enhanced above normal values because of the compressional heating resulting from the stream-stream interaction. The interface was crossed ~0520 UT on 9 March 2008. At the same time, IMF Bz turned northward, and Bx changed direction from sunward to antisunward. The AL index suddenly decreased from ~503 nT to ~-1301 nT in 10 min. The recovery phase of the storm began after the stream interface.

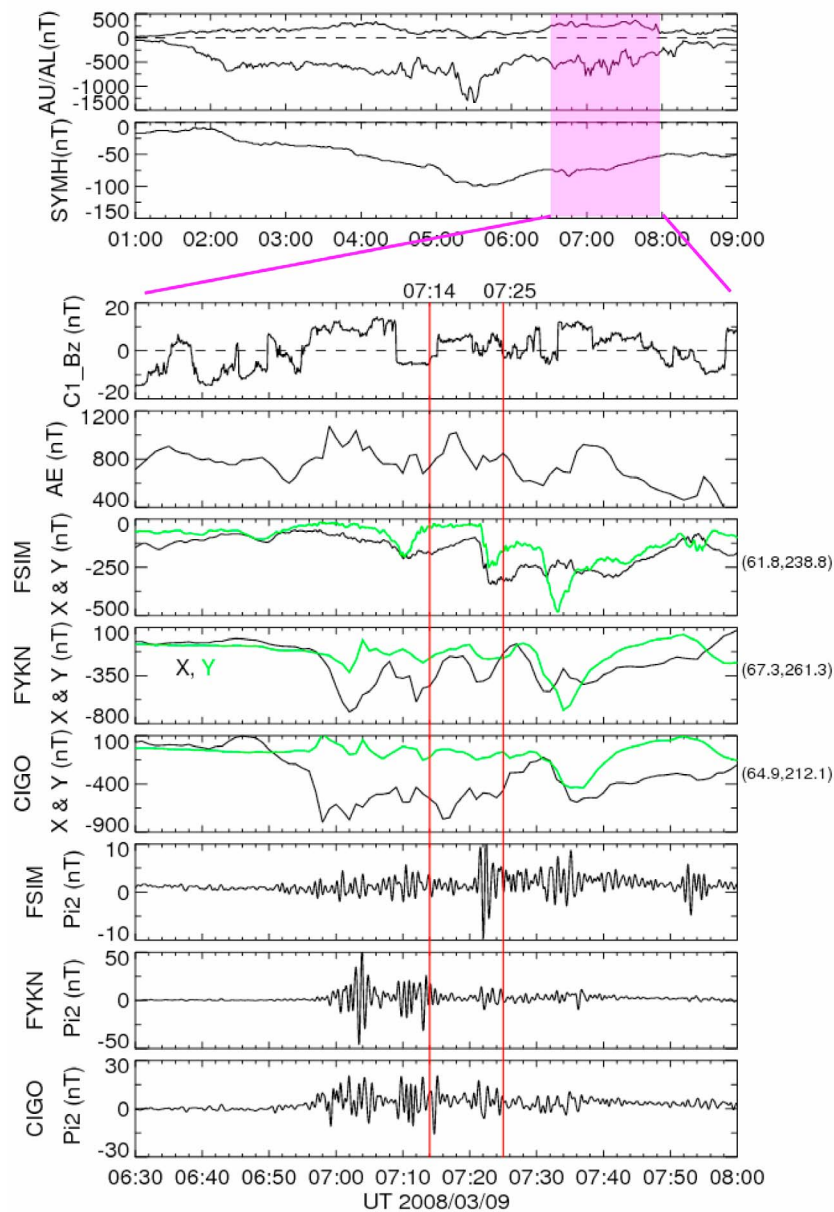


Figure 4. Geomagnetic index AL/AU and $SYM-H/ASYD$ during the interval 0100–0900 UT on 9 March 2008 (first and second panels). IMF Bz from Cluster C1 (third panel), AE (fourth panel), the ground-based magnetogram from Fort Simpson (FSIM), Fort Yukon (FYKN), and College International Geophysical Observatory (CIGO) stations (fifth through seventh panels), and Pi2 pulsations (eighth through tenth panels), during the interval of 0630–0800 UT.

[13] In Figure 4, the first and second panels show the geomagnetic index AL/AU and $SYM-H/ASYD$ during the interval 0100–0900 UT on 9 March 2008. The third panel of Figure 4 shows the interplanetary magnetic field (IMF) Bz observed by Cluster C1 for the interval of 0630 ~ 0800 UT on 9 March 2008. The IMF Bz fluctuated between -15 and 15 nT. The Alfvén waves in the solar wind are prominent during this interval. The fourth panel of Figure 4 shows the AE index for the interval of 0630 ~ 0800 UT. The fifth through seventh panels show the X and Y components of the geomagnetic field from the ground-based stations FSIM (61.8°N , 238.8°E), FYKN (67.3°N , 261.3°E), and CIGO (64.9°N , 212.1°E),

and their Pi2 pulsations are shown in the eighth through tenth panels. The AE index shows that onsets/reintensifications occurred during 0650 UT to 0750 UT. The westward electrojet estimated by the Bx and By at CIGO is stronger than that at FSIM and FYKN. Three Pi2 pulsation onsets were determined at the times of the first peak in signal amplitude above background, at 0658 UT, 0709 UT, and 0721 UT, for the three stations, respectively. The all-sky images from several stations of the THEMIS all-sky cameras [Mende *et al.*, 2008] also show the brightening and polar expansion of aurora corresponding to sharp enhancements of AE . Thus multiple substorm onsets/reintensifications occurred during

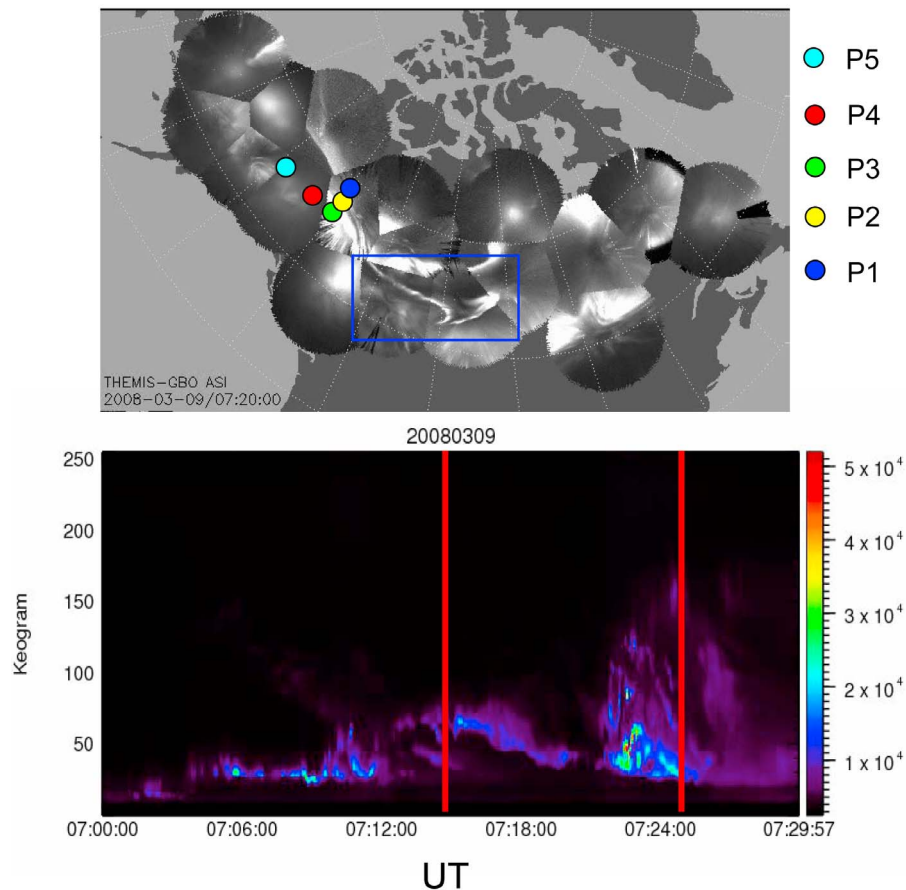


Figure 5. THEMIS all-sky camera observations at 0720 UT: (top) the footprints of THEMIS and (bottom) keogram from FSIM during 0700–0730 UT on 9 March 2008. The two red vertical lines mark the period of tailward flows observed by THEMIS. The blue box marks the auroral arc.

the interval 0655–0740 UT. Here we initially use the time of the Pi2 onsets as the substorm onset time.

[14] In this paper we are mainly interested in the tailward flow interval between 0715 and 0725 UT. Figure 5 (top) shows the THEMIS all-sky camera observations at ~0720 UT on 9 March 2008. The foot points of THEMIS are shown by colored circles. Figure 5 (bottom) shows the keogram from FSIM during 0700 ~ 0730 UT. The arc (marked by a blue box) developed a narrow streamer that moved westward along the latitude circle of $\sim 65^\circ$ during 0700 ~ 0721 UT, and the auroral streamer spread to polar region as discrete aurora after ~ 0721 UT. These processes can be clearly seen in the keogram and all-sky imager movies. The streamer is near the latitude of the CIGO station. At this time, the foot points of THEMIS probes traced using the T96 model [Tsyganenko and Stern, 1996] were located equatorward of the auroral streamer. The auroral streamer is usually related to a BBF [Nakamura *et al.*, 2001]. Therefore, these observations show a substorm with an associated tailward flow observed by THEMIS.

2.1. P5 Observations in the Rebound Region

[15] THEMIS P5 was closest to the Earth near $[-7.6, 5.6, -1.6] R_E$ at 0718 UT. Figures 6a and 6b show the keogram from FSIM and Pi2 observations both from FSIM and from

FYKN. The Pi2 pulsations can be used as a monitor for substorm onset, and the keogram shows the boundary of the aurora. Through the tailward flow interval FYKN (red line) Pi2 commenced at $\sim 0715:30$ UT, FSIM (black line) Pi2 started at 0721:30 UT. The brightening/expansion of the aurora correspond well to the starting times of the Pi2 pulsations.

[16] Figure 6c shows the ion velocity observed by P5, where the blue, green, and red lines represent V_x , V_y , and V_z , respectively. The prolonged tailward flow was observed from 0715:30 UT to 0721:30 UT. The maximum tailward flow velocity was 347 km s^{-1} . One minute before the beginning of the tailward flow at 0715:30 UT, a large V_y -component ($\sim 400 \text{ km s}^{-1}$) flow enhancement occurred, which stayed enhanced during the first part of the tailward flow. This duskside flow was mainly perpendicular to the background magnetic field as shown in Figure 6j. It might be related to the convection ($\mathbf{E} \times \mathbf{B}$) in the plasma sheet. After 0715:30 UT, the number density of ions decreased. Further, the ion velocity was decomposed into two components, where one was parallel to the magnetic field, (V_{\parallel}), and the other perpendicular (V_{\perp}). During the interval 0715 ~ 0721 UT, V_{\parallel} was dominant so that the tailward flow was nearly field-aligned. Although there was a large V_y component ($\sim 300 \text{ km s}^{-1}$) at 0714 ~ 0716 UT, it was most likely

P5 (THA)

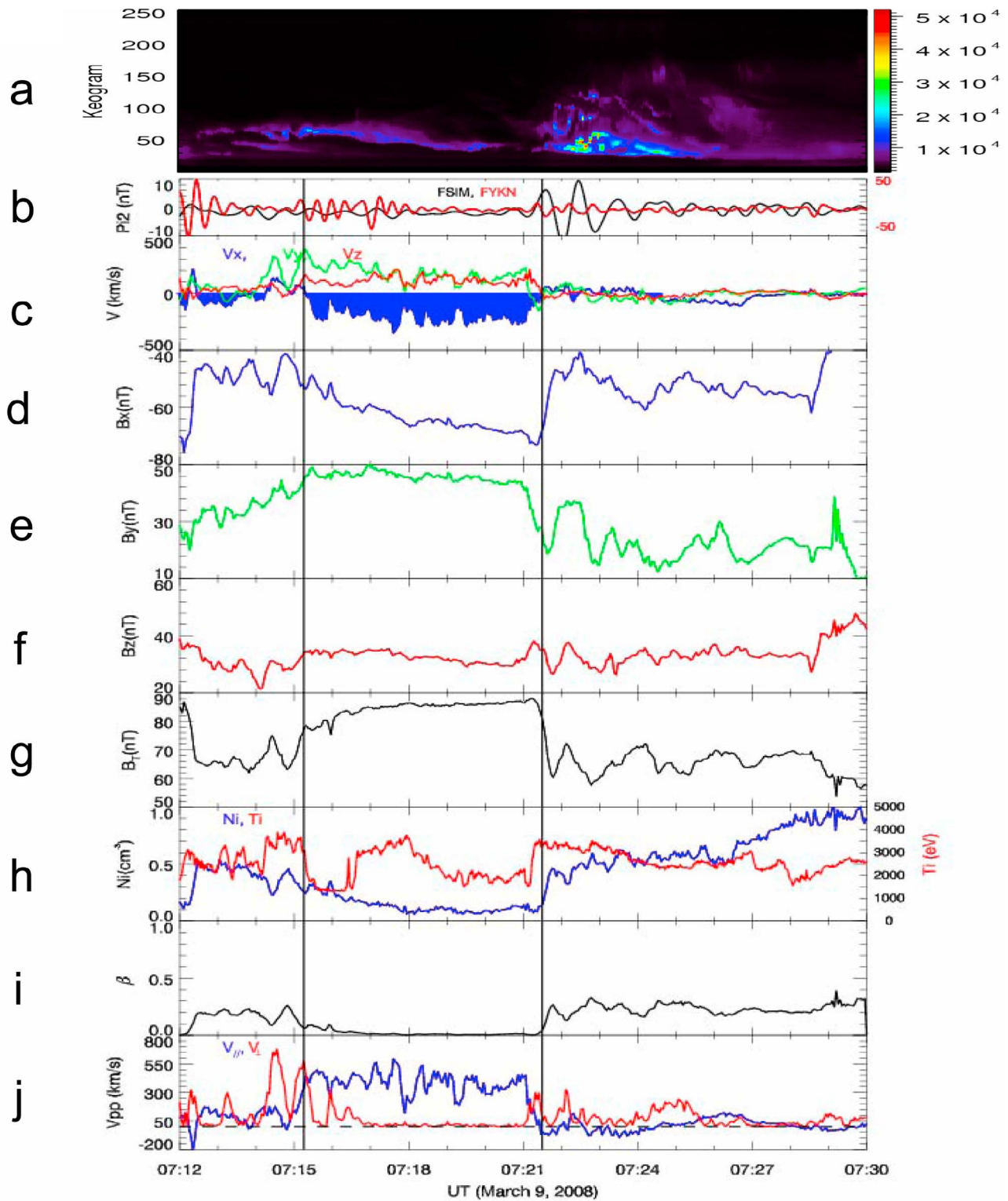


Figure 6. (a–j) Keogram and Pi2 and P5 observations of the ion velocity, magnetic field, ion density, ion temperature, plasma beta, and $V_{||}$ and V_{\perp} during 0712~0730 UT on 9 March 2008.

the effect of the configuration of tail (a large B_y), and was not caused by convection ($\mathbf{E} \times \mathbf{B}$).

[17] In this paper, the PSBL is identified by the large B_x , lower ion density $<0.3 \text{ cm}^{-3}$ and plasma beta <0.3 , $\sim \text{keV}$ ions, and dominant parallel velocity for the ion flow. Figures 6d–6g show the X , Y , and Z components (B_x , B_y , B_z) and the magnitude (B_T) of the magnetic field for P5, respectively. Note that the magnitude of B_x component was quite large throughout the interval (Figure 6d). P5 recorded an increase of B_x and a slight decrease of B_y and B_z . This is consistent with thinning of the plasma sheet, which usually occurs during the growth phase of substorms. As shown in Figures 6h and 6i, the ion density was $\sim 0.13 \text{ cm}^{-3}$, the temperature $\sim 2\text{--}3 \text{ keV}$, and $\beta \sim 0.01$ between 0715 and 0721 UT. These parameters identified that P5 was located in the outer part of the PSBL [Baumjohann *et al.*, 1988, 1989].

[18] In addition, the time-energy spectrograms of the ion and electrons (not shown in this paper) display that the electrons were around $\sim 1 \text{ keV}$, and the ions around 2 keV . It was a more structureless and thermalized ion population without an extended dispersed ion structure.

[19] The tailward flow observed by P5 ceased at $\sim 0721 \text{ UT}$. At this time, a Pi2 commenced at FSIM and the aurora expanded poleward. This indicates another substorm onset. $|B_x|$ and B_y sharply decreased, and B_z suddenly increased. The ion density and temperature increased as well. These features of the magnetic field and plasma can be identified as either magnetic field dipolarization or the entering of P5 into the CPS.

2.2. P4 and P3 Observations

[20] Figure 7 shows an overview plot of P4 located at $[-10.7, 4.5, -1.9] R_E$. Figure 7 has the same format as that in Figure 6. The tailward flow with a maximum of $\sim 250 \text{ km s}^{-1}$ was observed during the interval 0714–0724 UT, the first 7 min fast flow and the last 3 min slow flow. P4 observed a large $B_x \sim -60 \text{ nT}$ and large $B_T \sim 70 \text{ nT}$. During the interval of the tailward flow, the ion density decreased from $\sim 0.4 \text{ cm}^{-3}$ to $\sim 0.1 \text{ cm}^{-3}$, and minimum ion temperature $\sim 1.6 \text{ keV}$ and $\beta \sim 0.02$ place P4 in the PSBL. For the fast flow between 0714 and 0721 UT, the parallel velocity was dominant except for a perpendicular velocity pulse at 0721 UT, whereas V_{\parallel} was similar to V_{\perp} for the slow flow in the interval of 0721–0724 UT.

[21] It is also interesting to note the variations of magnetic field accompanying the tailward flow. During the interval of 0714–0720 UT, B_x decreased from -50 nT to $\sim -60 \text{ nT}$, B_y decreased from 35 to 20 nT, B_z decreased from 15 to 5 nT, and B_T increased by $\sim 10 \text{ nT}$. The increase of $|B_x|$ and decrease of B_z indicate a stretching of the magnetotail. In this interval, P4 was closer to the outer boundary of the PSBL with the lobe. All of these features indicate that the flow is faster in the outer part of the PSBL close to the lobe. Following the Pi2 enhancement and the auroral polar expansion after $\sim 0720 \text{ UT}$, the magnetic field dipolarization began and the tailward flow decayed.

[22] In Figures 8a and 8b, the time-energy spectra show a limited range of the spectrum for ion (between $\sim 1 \text{ keV}$ and $\sim 10 \text{ keV}$) and electron (between $\sim 300 \text{ eV}$ and $\sim 3 \text{ keV}$) during the tailward flow interval (marked by two vertical red lines). Figures 8c and 8d present pitch angle distributions (PAD) of ESA ions and electrons, obtained by P4 between

0700:02 and 0729:59 UT. P4 detected monodirectional electrons and ions PAD of high-energy electrons during the tailward flow interval (indicated by two vertical red lines). In Figure 8e, the velocity distributions of ions show a tailward/duskward streaming component during the period of the tailward flows. The time-energy spectrum is a more structureless, thermalized ion population, which does not show an extended dispersed ion structure of beamlets. In addition, no counterstreaming ions are observed.

[23] P3 and P4 were separated by 887, 6062 and 589 km in X , Y , and Z , respectively. As shown in Figure 2, the tailward flow at P3 was delayed by $\sim 5 \text{ min}$ compared to that of P4. The magnitudes of B_x and B_T at P3 are less than that at P4 as shown in Figure 9; thus P3 was closer to the CPS than P4. The tendency of the variations of B_x from P3 (Figure 9) was similar to those at P4 (Figure 7), while the tendencies of B_y and B_z are counter to those at P4.

[24] For P3, the tailward flow appeared between 0719 and 0724 UT, when the ion density, the ion temperature and plasma- β decreased to $\sim 0.18 \text{ cm}^{-3}$, $\sim 2 \text{ keV}$, and ~ 0.02 , respectively. An explanation for their decline could be the thinning of the CPS leading to P3 moving deeper into the PSBL. The tailward flow at P3 is made up of two parts: intervals 1719–1721 UT and 1722–1724 UT. For the first part V_{\parallel} was dominant. The first part of the tailward flow in the interval of 1719–1721 UT is caused by the former substorm onset at 0715 UT, and it is assumed that the same flow as observed by P5 and P4 is seen. At 0721 UT the aurora expanded poleward followed by a Pi2 onset, the velocity of the tailward flow decreased, then $\sim 1 \text{ min}$ later the tailward flow enhanced again. V_{\parallel} was similar to V_{\perp} for the second part. Although B_x increased, the plasma- β kept very low in this interval. From the variations of B_x and B_z , a dipolarization occurred at around 0721 UT. Indeed, the second part of the tailward flow from 0721 UT to 0724 UT is related to the second substorm onset at 0721 UT.

2.3. P2 Observations

[25] P2 was located at $[-14.6, 4.5, -2.1] R_E$. The format of Figure 10 is identical to that of Figure 6. The tailward flow with a maximum of $\sim 128 \text{ km s}^{-1}$ was detected by P2 during the interval 0717–0724 UT. B_x and B_T have large magnitudes with maxima of 50 nT and 60 nT, respectively. The V_{\parallel} was dominant. During the tailward flow interval, the ion density, temperature and β decreased to $\sim 0.18 \text{ cm}^{-3}$, $\sim 2 \text{ keV}$, and 0.07, respectively. The electron energy was distributed between 300 eV–3 keV, and the ion energy was mainly between 1–20 keV.

[26] With the enhancement of the tailward flow, the negative B_x decreased to $\sim -48 \text{ nT}$, the positive B_y increased to $\sim 25 \text{ nT}$, and the positive B_z increased to $\sim 5 \text{ nT}$ then dropped down. It indicates the thinning of the current sheet. It looks like the magnetotail characteristic during the growth phase of substorms.

[27] It is worth noting that V_x changed from tailward (<0) to earthward (>0) at $\sim 0724 \text{ UT}$. This earthward flow ($\sim 100 \text{ km s}^{-1}$) was also observed by P3 at least 1 min later. P3 and P2 were separated about $\sim 3.7 R_E$ in the X direction. If the earthward flow propagated from P2 to P3, the estimated average speed of the earthward flow would be $\sim 400 \text{ km s}^{-1}$, which is much higher than the observed speed.

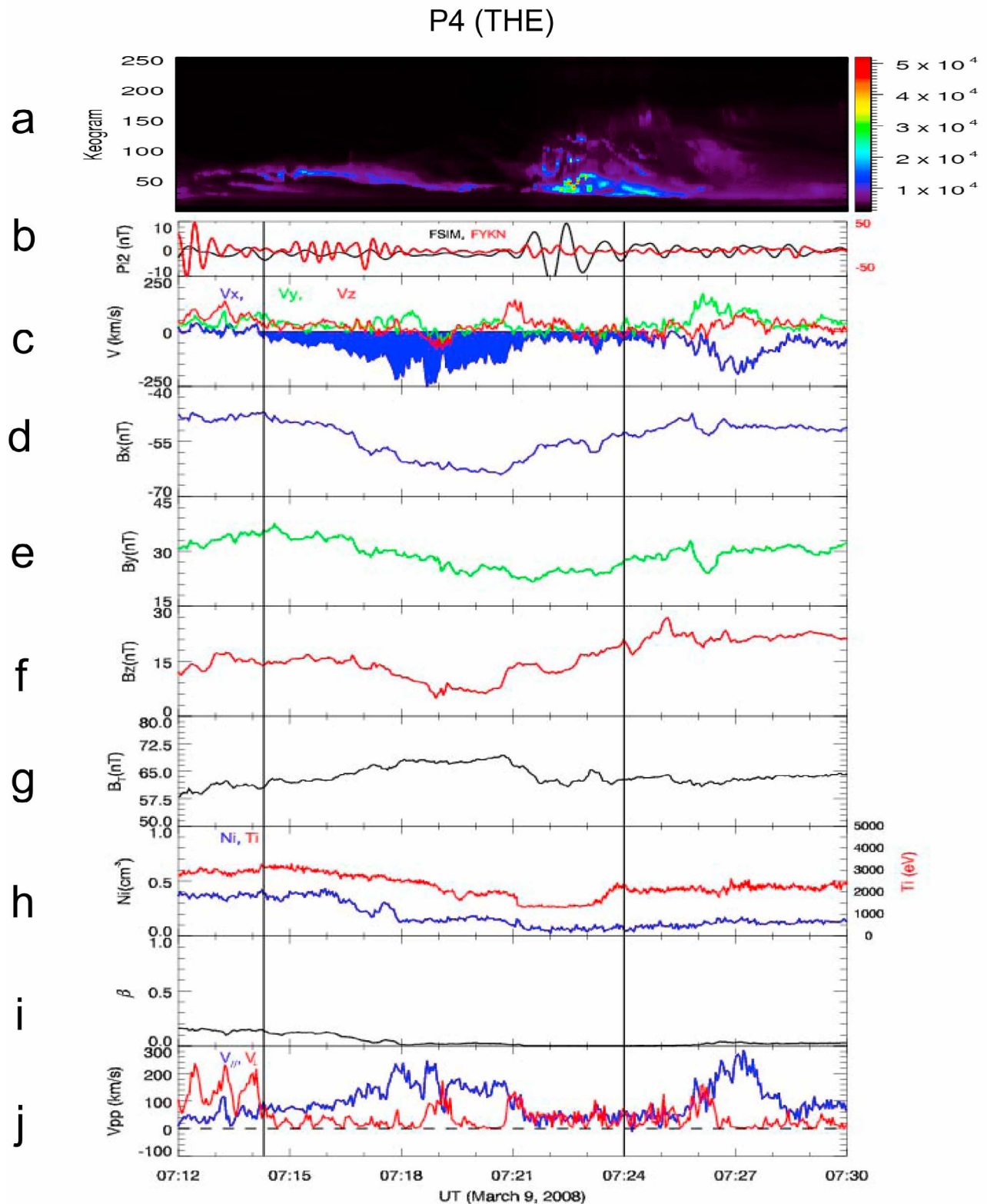


Figure 7. (a–j) Identical to Figure 6 but for observations of P4.

2.4. P1 Observations

[28] P1 was located at $[-17.6, 4.8, -1.2] R_E$ at 0718 UT. As shown in Figure 11, the tailward flow with a maximum of 244 km s^{-1} was detected by P1 during the

interval of 0718 ~ 0725 UT. Several plasma sheet crossings were identified where $B_x = 0$ and B_T has a minimum [Zhang *et al.*, 2002, 2005; Rong *et al.*, 2010]. The high ion density, ion temperature and large β (>1) during the tailward

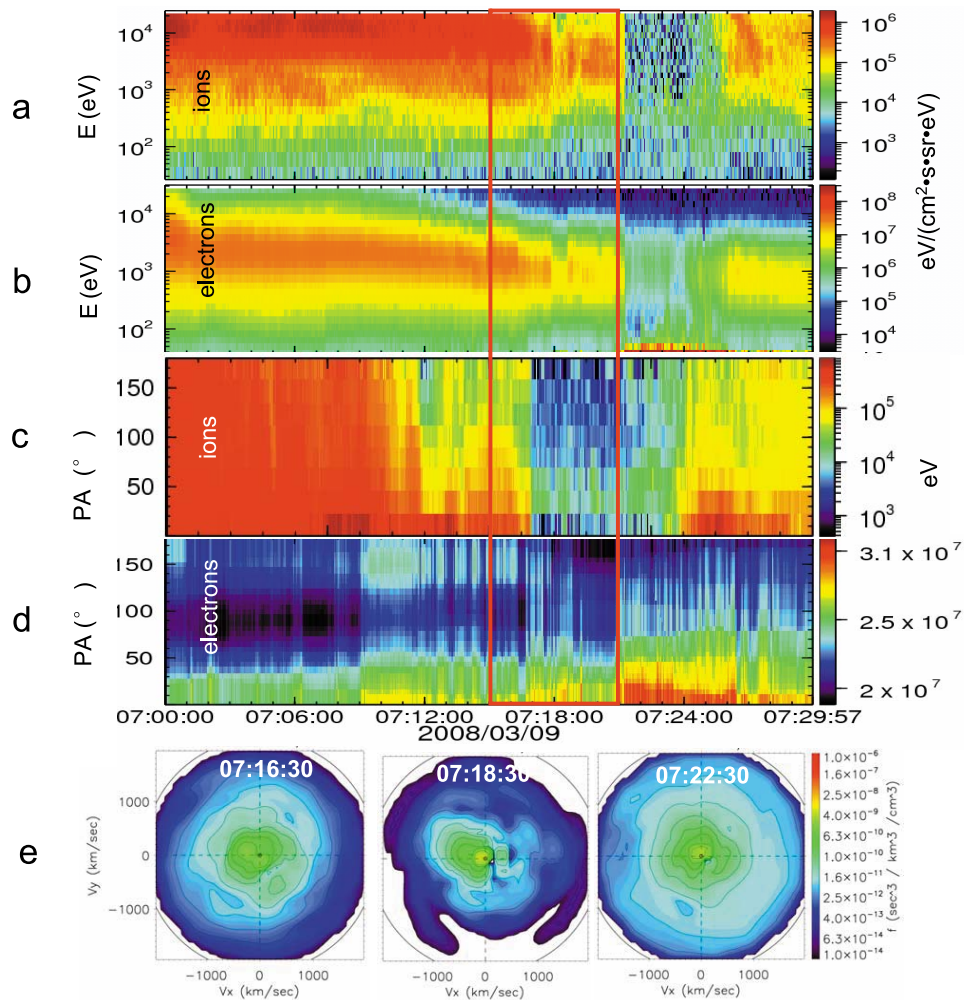


Figure 8. (a, b) Time-energy spectrograms of the ions and electrons, (c, d) the pitch angle of ions and electrons, and (e) the ion velocity distributions observed by P5 on 9 March 2008. The red box indicates the period of the tailward flow observed by P5.

flow interval indicate that P1 was located in the plasma sheet.

[29] The tailward flow started at ~ 0718 UT. The total magnetic field, B_T , dropped to around zero at 0722:13 and 0723:49 UT, respectively. A negative-to-positive B_x and a positive-to-negative B_z signature was observed for the first crossing of the neutral sheet, the detail will be discussed in section 3.3. One minute later, B_z gradually turned to north from south and B_x decreased gradually to zero then increased keeping a positive value (earthward) while B_T had a similar variation as B_x around 0723:49 UT.

2.5. Variations of the Total Pressure and the Relationship Between V_x and Plasma- β

[30] Figure 12 shows the thermal, magnetic, and total pressure of plasma for the five probes of THEMIS during the interval 1700 \sim 1730 UT. Figure 12 shows that the magnetic pressure was dominant and that the total pressure decreased from P5 to P1.

[31] We order the fast flow velocity V_x by beta, which indicates the relative location of the plasma sheet. Figure 13a gives the variations of V_x with the plasma- β observed by

four THEMIS probes from P5 to P2 during the interval 1700 \sim 1730 UT on 9 March 2008. It is noted that the tailward flows ($V_x < 0$) are dominant for the lower plasma- β . For medium β , either the tailward or earthward flows are observed. For relatively high β , the earthward flows are dominant. The corresponding β values that separate the flows are different for the four probes.

3. Discussion

3.1. Tailward Flows in the PSBL

[32] The IMF B_z and the substorm activities were very complex for this tailward flow event on 9 March 2008. The prolonged tailward flows continued for ~ 10 min and extended over $\sim 10 R_E$ along X . As shown in Figures 6, 7, and 9, the ion density, ion temperature and plasma beta quickly decreased and kept a lower level (at values typical in the PSBL [Baumjohann *et al.*, 1988, 1989]) when the tailward flows got enhanced. We must mention that the PSBL is identified by the strong magnetic field ($B_x/B_z > 2$), lower ion density $< 0.3 \text{ cm}^{-3}$ and plasma beta < 0.3 , $\sim \text{keV}$ ions, and dominant parallel velocity for the ion flow. The storm con-

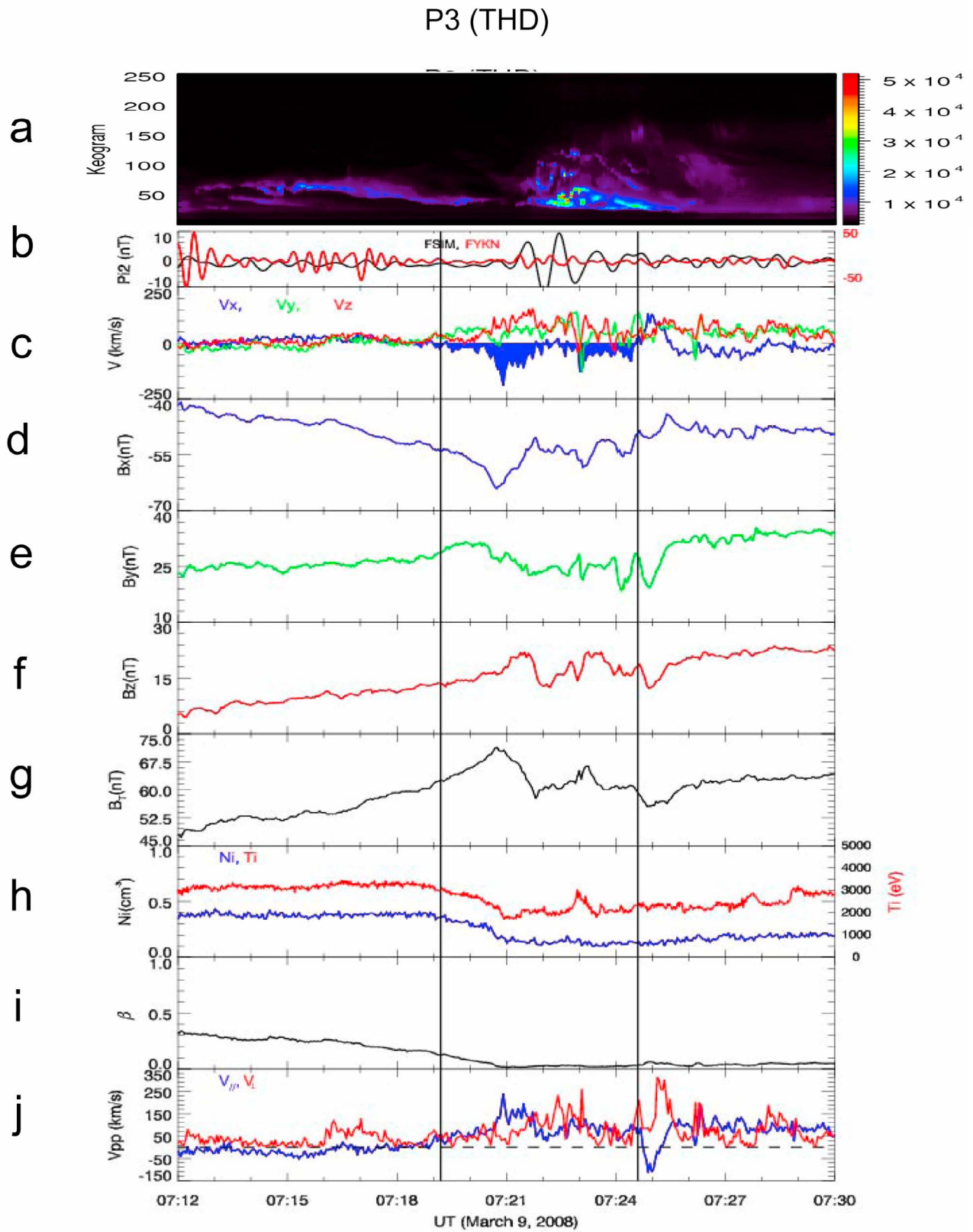


Figure 9. (a–j) Identical to Figure 6 but for observations of P3.

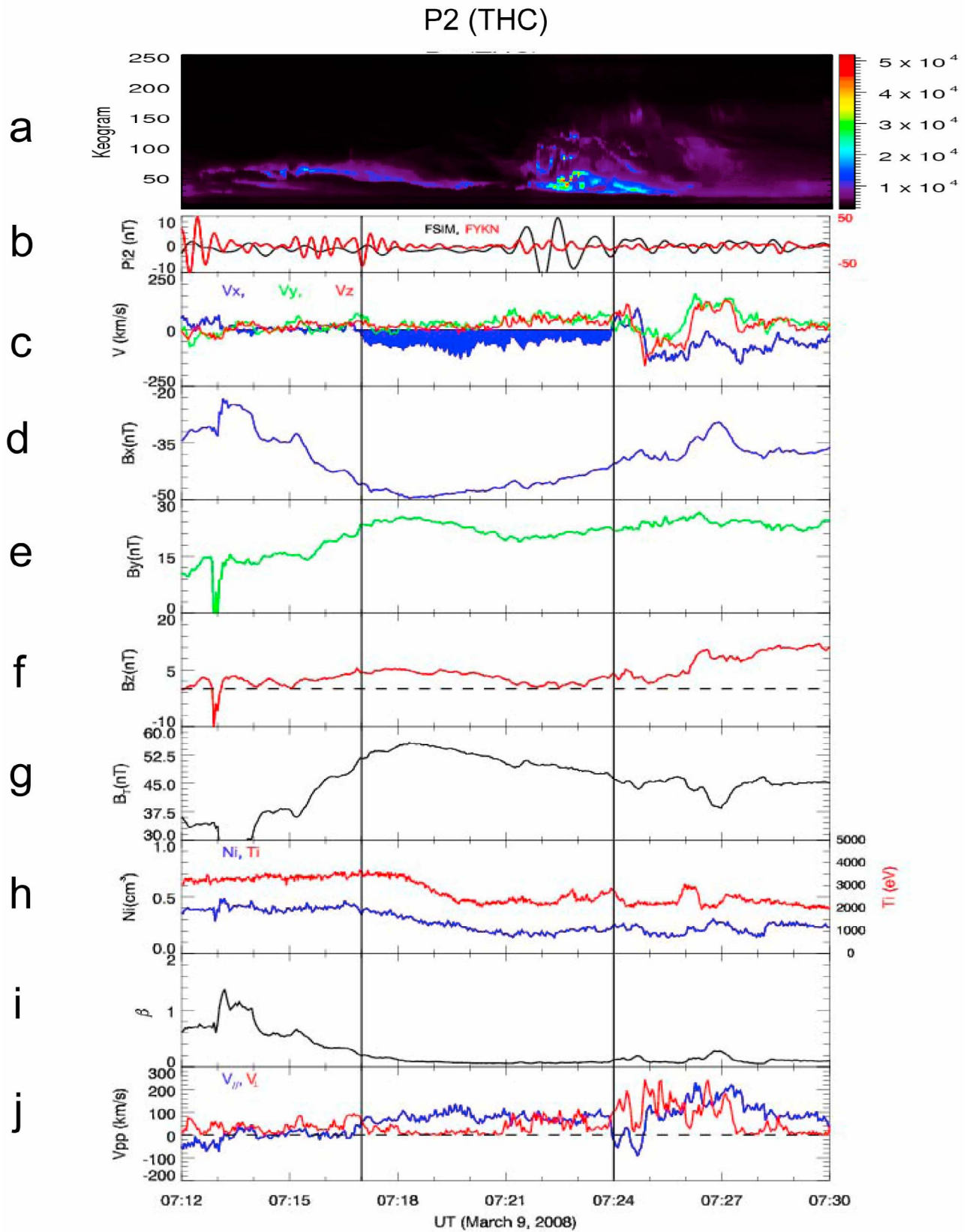


Figure 10. (a–j) Identical to Figure 6 but for observations of P2.

P1 (THB)

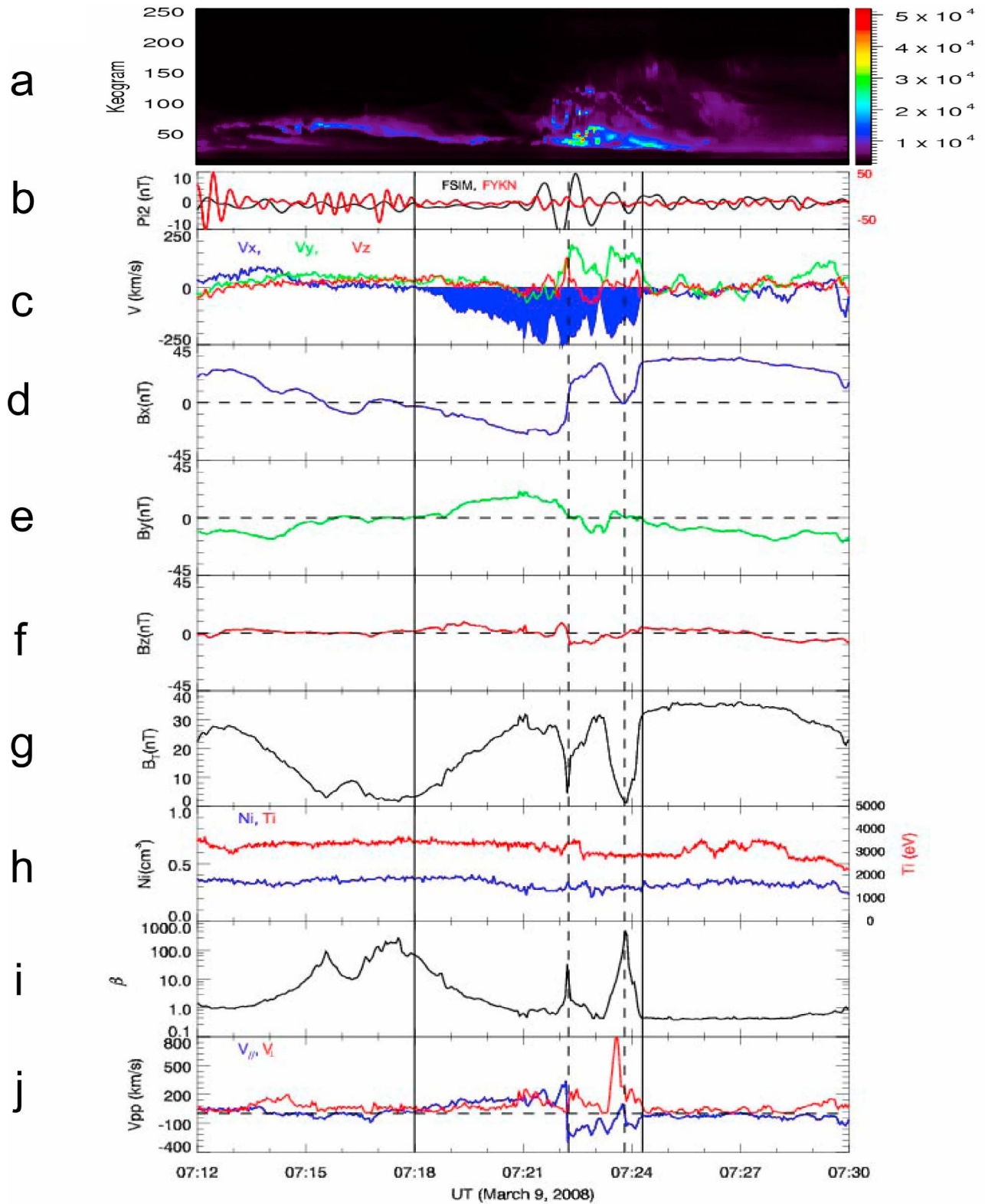


Figure 11. (a–j) Identical to Figure 6 but for observations of P1. The vertical dashed lines indicate the quasi-zero points of the magnetic field observed by P1.

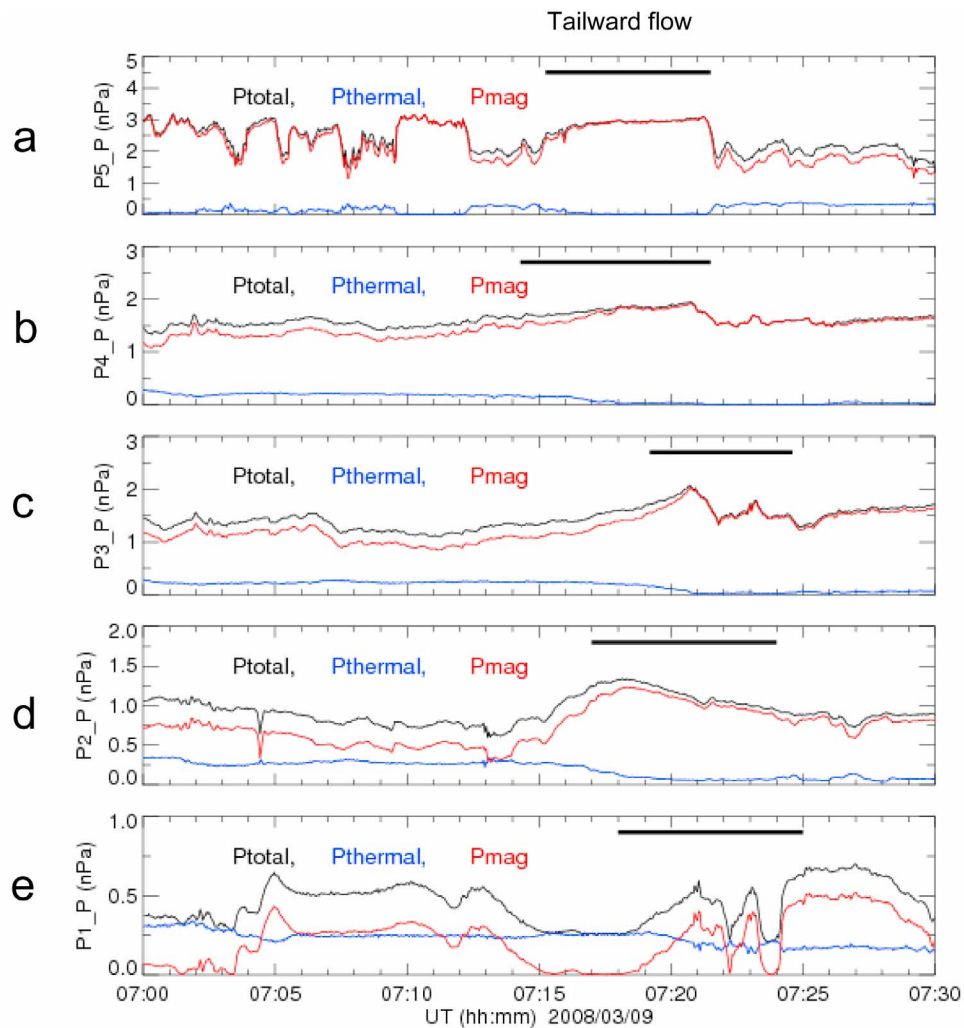


Figure 12. (a–e) Thermal, magnetic, and total pressure by five probes of P5–P1 during 0700 ~ 0730 UT on 9 March 2008.

dition makes the tail condition quite special. What is interesting in this event is that the persistent tailward flow (not a beam, from checking the distribution function) at the boundary and its changes correspond to auroral/electrojet reactivation. At the first stage of tailward flow increase, the magnetic field lines were stretched and the magnetic flux increased for all spacecraft except for P2. This indicates that the spacecraft moved to the outer boundary of the PSBL. Indeed, the tailward flows could be closer to the lobe. However, this would not be consistent with the expected occurrence of fast flows during plasma sheet expansions [Lui *et al.*, 1978], because this event on 9 March 2000 occurred during multiple onsets. The substorm features were buried in the high-intensity continuous *AE* index activity during the recovery phase of the storm on 9 March 2008.

[33] The flow characteristics also changed significantly along the *Z* axis as also shown by Baumjohann *et al.* [1988]. The spatial scale of the PSBL is on the order of 0.2–0.5 R_E [Ashour-Abdalla *et al.*, 2008]. In this paper, the thickness of the PSBL was not really observed. P3 was closer to the CPS than P4, but the tailward flow observed by P4 was earlier than that at P3. It may be worth to note that comparing the

location of P4 (–10.7, 4.5, –1.9) R_E with P3 (–10.9, 3.6, –1.8) R_E there is only a larger separation of 0.9 R_E in *Y* direction. But the observed flow by P3 is much different from that observed by P4. A substorm expansion onset occurred obviously at ~0721 UT. However, dipolarization of the magnetic field occurred at 0721 and 0723 UT for P4 and P3, respectively, during substorm expansion phase. The intense tailward flow at P4 occurred mainly during the growth phase of substorm with stretched magnetic configuration. But there was still enhanced tailward flow in the two dipolarization processes. Tailward flow at P3 enhanced only during two dipolarization processes. On the other hand, the V_z suddenly increased at two dipolarization times while V_{\perp} intensified so that flow is no longer field-aligned. It could be possible that P4 was approaching the flow region in the PSBL while the P3 missed it at the beginning. The observation of tailward flow by P1 is similar to that by P4 with a time delay. P5 is similar to P4 during the growth. P2 observed weaker flow but no clear dipolarization, which may arise from its lower location in *Z* coordinate ($Z = -2.1 R_E$) taking it further away from the neutral sheet. The characteristics mentioned above indicate that generation of tailward

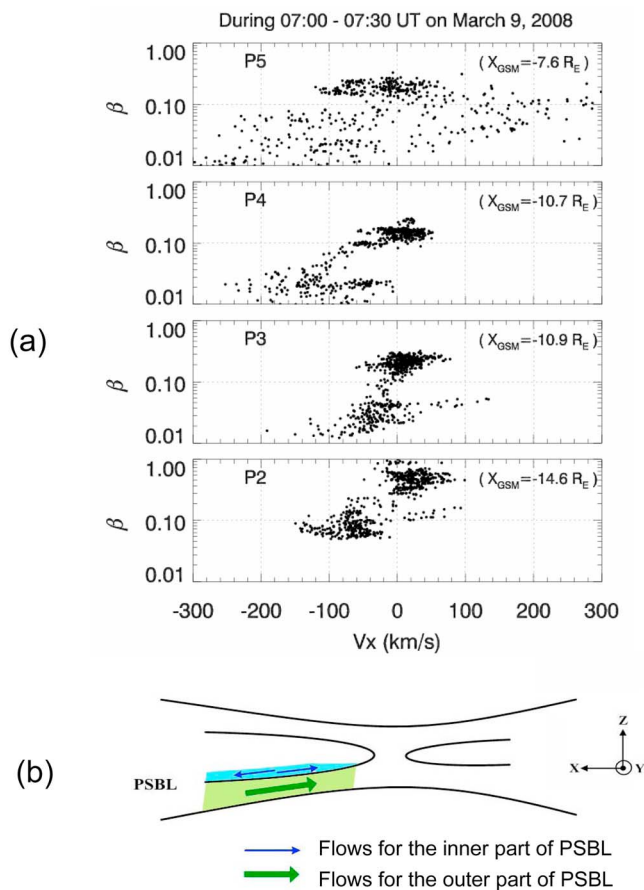


Figure 13. (a) Distribution of V_x as a function of plasma- β during the interval of 1700 ~ 1730 UT. (b) A sketch of the plasma flows in the open and closed field line regions in the X - Z plane.

flow may closely depend on the configuration of magnetic field associated with substorms. Indeed, *Ashour-Abdalla et al.* [2008] clearly show that the shape of the PSBL is irregular and modeled by large-scale solar wind/magnetosphere interaction.

3.2. Possible Generation Mechanism of Tailward Flows

[34] It is well known that the occurrences of multiple onsets are often accompanied by earthward flows in the CPS, which are called BBFs [e.g., *Baumjohann et al.*, 1990; *Angelopoulos et al.*, 1992; *Nakamura et al.*, 2004; *Cao et al.*, 2006]. *Panov et al.* [2010a] showed for the first time the rebound of BBFs, observed by the THEMIS probes in the plasma sheet. Here we observe tailward flow in the PSBL. The maximum speed of the tailward flow was observed by P5, which was closest to the Earth. The flow extended over $\sim 10 R_E$ and entered into the plasma sheet near P1 at $X \sim -17.6 R_E$.

[35] Some previous observations attributed the tailward flows in the PSBL to the contribution of counterstreaming beams produced by near-Earth mirroring of ion beams [*Williams*, 1981; *Forbes et al.*, 1981; *Eastman et al.*, 1984; *Lennartsson et al.*, 2009]. In fact, earthward flow ($V_x > 0$) was observed by all five probes prior the occurrence of the tailward flow, in particular, they are clearest in P5 and P1. However, the persistent tailward flow in this event was not a beam, from checking the distribution function. As illustrated

in Figure 13b (based on the interpretation of Figure 13a), the ion flow is tailward for the outer part of the PSBL and earthward/tailward for the inner PSBL. This phenomenon was also supported by the pitch angle distributions (PAD) of ESA electrons (only P4 shown in this paper).

[36] Our observations are consistent with the simulation results by *Birn et al.* [2004], who found that tailward flows developed in the PSBL when the earthward flows were close to the Earth. This is clearly visible in Figure 5 of *Birn et al.* [2004], which shows that [*Birn et al.*, 2004, p. 1776], “At the later time after the depletion of a flux tube, the tailward flow develops on the outside of the bubble, which increases in speed as the earthward flow becomes reduced. This flow fills the void left behind by the earthward moving bubble.” Figure 12 shows that the magnetic pressure was dominant for all time and the total pressure decreased from P5 to P1. The magnetic pressure might affect the propagation of the tailward flows.

[37] In fact, there are three possible kinds of tailward flow generation discussed in this paper: (1) *Birn et al.* [2004] tailward flow (flow filling the void region), (2) bouncing of earthward flow due to interaction with the inner magnetosphere, and (3) reconnection-related flows assuming a reconnection site earthward of the spacecraft [*Ashour-Abdalla et al.*, 2002, 2009; *El-Alaoui et al.*, 2009]. The main difference among the spacecraft comes from the fact that different spacecraft observed different types of flows. Here, types 1 and 2 are actually difficult to distinguish. The flux tube motion [*Panov et al.*, 2010a, 2010b] was not directly observed. Nevertheless, it is possible that all flows are related to reconnection (or activation of flux transport) as discussed below.

[38] As shown in Figure 4, *AE* and *CIGO-Pi2* suddenly enhanced at ~ 0714 UT. A negative bay was also observed by west of the spacecraft foot points. Note that this onset at ~ 0714 UT happened at the same time as the tailward flows started in P4 and P5, which are the westernmost spacecraft. During the interval of ~ 0718 – 0719 UT a strong perpendicular flow component was observed by P4, which coincided with the start of the tailward flow at P1, and P2 pressure decrease. The P2 flux decrease suggests some activation of reconnection possibly transporting magnetic flux earthward. This might be connected to the bouncing flow observed by P5 and P4.

[39] It is quite unusual to observe such prolonged tailward flows at that location. Because the event was within a major storm, the distinction of the specific observations from other nonstorm observation. The solar wind velocity ($\sim 550 \text{ km s}^{-1}$) smoothly increased, and the proton density was high ($\sim 15 \text{ cm}^{-3}$). The IMF B_z fluctuated between -15 and 15 nT . In these conditions, the magnetotail would be continually stretched, and the near-Earth neutral line might be formed [*Miyashita et al.*, 2004]. The simulations of *Birn et al.* [2004] show the tailward flows developed after the depletion of a flux tube. Thus, the storm time tailward flows in the PSBL would be investigated in further.

3.3. Tailward Flows Related to an X Line

[40] P1 stayed in the southern hemisphere of the plasma sheet before 0722 UT, and the tailward flow resulted from filling of the flows in the PSBL observed by the four probes of P5 to P2. Two null points with the reversal of the B_x and

B_z (see Figure 11) were detected by P1 at 0722:13 and 0723:49 UT. The first null event at is a typical O line. The second null might be an X line, since the V_x seems to have short minimum and is also closer to the turning point of the flow from the negative to positive. The X line is earthward of P1. At any rate, flow at P1 is most likely showing V_x related to the reconnection region. Note that P3 and P4 have large positive V_z , here gives an enhanced E_y , possibly seeing the inflow toward X line. Thus the tailward flow during the interval from 0722 to 0725 UT was a result of the new X line. Observations of the aurora, Pi2 pulsations and the negative bays established that a substorm expansion phase was going on during this period. This substorm activity changed the configuration of the magnetotail, and resulted in variations of the tailward flows observed by five probes of THEMIS at different regions.

4. Summary

[41] In this paper, we present an event of the tailward flows observed by THEMIS from $X \sim -7.6$ to $-17.6 R_E$ in the PSBL. The flows lasted about 10 min. During the tailward flow interval, the ion density, ion temperature, and ion/electron spectrum clearly showed the characteristics of the outer part of the PSBL. The high-speed flows mainly propagated along field lines. The field-aligned tailward flows in the PSBL are consistent with the simulation results [Birn *et al.*, 2004]. The tailward flows in the PSBL may be referred to the contribution of the bounced flows of the earthward flows in the CPS. Observations demonstrate that the tailward flows were closely related to the substorms, which occurred successively during the storm. The successive substorms during the storm enable favorable conditions for a near-Earth reconnection region as well as strong bursty bulk flow, enabling favorable conditions for tailward flows.

[42] **Acknowledgments.** We appreciate discussions with M. Fujimoto and V. S. Semenov. We acknowledge the CDAWeb for access to the ACE and Cluster data. THEMIS is supported in the United States by NASA contract NAS5-02099. The AL data are provided by the World Data Center for Geomagnetism at Kyoto University. We thank J. W. Bonnell and F. S. Mozer for use of EFI data, D. Larson and R. P. Lin for use of SST data, S. Mende and E. Donovan for use of the ASI data, the CSA for logistical support in fielding and data retrieval from the GBO stations, I. Mann for use of the GMAG data, and the CSA for support of the CARISMA network. This work was supported by an NSFC grant (41031066) and by the Ocean Public Welfare Scientific Research Project, State Oceanic Administration, China (201005017).

[43] Masaki Fujimoto thanks the reviewers for their assistance in evaluating this paper.

References

Angelopoulos, V. (2008), The THEMIS mission, *Space Sci. Rev.*, *141*, 5–34, doi:10.1007/s11214-008-9336-1.

Angelopoulos, V., W. Baumjohann, C. F. Kennel, F. V. Coroniti, M. G. Kivelson, R. Pellat, R. J. Walker, H. Luhr, and G. Paschmann (1992), Bursty bulk flows in the inner central plasma sheet, *J. Geophys. Res.*, *97*, 4027–4039, doi:10.1029/91JA02701.

Angelopoulos, V., C. F. Kennel, F. V. Coroniti, W. C. Feldman, J. T. Gosling, M. G. Kivelson, R. J. Walker, and C. T. Russell (1993), Observations of a quasi-static plasma sheet boundary, *Geophys. Res. Lett.*, *20*, 2813–2816, doi:10.1029/93GL01979.

Angelopoulos, V., C. F. Kennel, F. V. Coroniti, R. Pellat, M. G. Kivelson, R. J. Walker, C. T. Russell, W. Baumjohann, W. C. Feldman, and J. T.

Gosling (1994), Statistical characteristics of bursty bulk flow events, *J. Geophys. Res.*, *99*, 21,257–21,280, doi:10.1029/94JA01263.

Ashour-Abdalla, M., M. El-Alaoui, F. V. Coroniti, R. J. Walker, and V. Peromian (2002), A new convection state at substorm onset: Results from an MHD study, *Geophys. Res. Lett.*, *29*(20), 1965, doi:10.1029/2002GL015787.

Ashour-Abdalla, M., J. M. Bosqued, M. El-Alaoui, V. Peromian, T. Umeda, and R. J. Walker (2008), Modeling PSBL high speed ion beams observed by Cluster and Double Star, *Adv. Space Res.*, *41*(10), 1598–1610, doi:10.1016/j.asr.2007.04.018.

Ashour-Abdalla, M., J.-M. Bosqued, M. El-Alaoui, V. Peromian, M. Zhou, R. Richard, R. Walker, A. Runov, and V. Angelopoulos (2009), A simulation study of particle energization observed by THEMIS spacecraft during a substorm, *J. Geophys. Res.*, *114*, A09204, doi:10.1029/2009JA014126.

Auster, H. U., et al. (2008), The THEMIS fluxgate magnetometer, *Space Sci. Rev.*, *141*, 235–264, doi:10.1007/s11214-008-9365-9.

Balogh, A., et al. (2001), The Cluster Magnetic Field Investigation: Overview of in-flight performance and initial results, *Ann. Geophys.*, *19*, 1207–1217, doi:10.5194/angeo-19-1207-2001.

Baumjohann, W., G. Paschmann, N. Scopke, C. A. Cattell, and C. W. Carlson (1988), Average ion moments in the plasma sheet boundary layer, *J. Geophys. Res.*, *93*, 11,507–11,520, doi:10.1029/JA093iA10p11507.

Baumjohann, W., G. Paschmann, and C. A. Cattell (1989), Average plasma properties in the central plasma sheet, *J. Geophys. Res.*, *94*, 6597–6606, doi:10.1029/JA094iA06p06597.

Baumjohann, W., G. Paschmann, and H. Luhr (1990), Characteristics of high-speed ion flows in the plasma sheet, *J. Geophys. Res.*, *95*, 3801–3809, doi:10.1029/JA095iA04p03801.

Birn, J., J. Raeder, Y. Wang, R. Wolf, and M. Hesse (2004), On the propagation of bubbles in the geomagnetic tail, *Ann. Geophys.*, *22*, 1773–1786, doi:10.5194/angeo-22-1773-2004.

Cao, J. B., et al. (2006), Joint observations by Cluster satellites of bursty bulk flows in the magnetotail, *J. Geophys. Res.*, *111*, A04206, doi:10.1029/2005JA011322.

Cowley, S. W. H., R. J. Hynds, I. G. Richardson, P. W. Daly, T. R. Sanderson, K.-P. Wenzel, J. A. Slavin, and B. T. Tsurutani (1984), Energetic ion regimes in the deep geomagnetic tail: ISEE 3, *Geophys. Res. Lett.*, *11*, 275–278, doi:10.1029/GL011i003p00275.

Du, A. M., B. T. Tsurutani, and W. Sun (2008), Anomalous geomagnetic storm of 21–22 January 2005: A storm main phase during northward IMFs, *J. Geophys. Res.*, *113*, A10214, doi:10.1029/2008JA013284.

Eastman, T. E., L. A. Frank, W. K. Peterson, and W. Lennartsson (1984), The plasma sheet boundary layer, *J. Geophys. Res.*, *89*, 1553–1572, doi:10.1029/JA089iA03p01553.

El-Alaoui, M., M. Ashour-Abdalla, R. J. Walker, V. Peromian, R. L. Richard, V. Angelopoulos, and A. Runov (2009), Substorm evolution as revealed by THEMIS satellites and a global MHD simulation, *J. Geophys. Res.*, *114*, A08221, doi:10.1029/2009JA014133.

Forbes, T. G., E. W. Hones Jr., S. J. Bame, J. R. Asbridge, G. Paschmann, N. Scopke, and C. T. Russell (1981), Evidence for the tailward retreat of a magnetic neutral line in the magnetotail during substorm recovery, *Geophys. Res. Lett.*, *8*, 261–264, doi:10.1029/GL008i003p00261.

Frank, L. A. (1976), Hot plasmas in the Earth's magnetosphere, in *Physics of Solar Planetary Environments*, vol. 2, edited by D. J. Williams, pp. 685–700, AGU, Washington, D. C.

Hones, E. W., Jr., J. Birn, S. J. Bame, G. Paschmann, and C. T. Russell (1982), On the three-dimensional magnetic structure of the plasmoid created in the magnetotail at substorm onset, *Geophys. Res. Lett.*, *9*, 203–206, doi:10.1029/GL009i003p00203.

Iyemori, T., and D. R. K. Rao (1996), Decay of the Dst field of geomagnetic disturbance after substorm onset and its implication to storm-substorm relation, *Ann. Geophys.*, *14*, 608–618, doi:10.1007/s00585-996-0608-3.

Kamide, Y., et al. (1998), Current understanding of magnetic storms: Storm-substorm relationships, *J. Geophys. Res.*, *103*, 17,705–17,728, doi:10.1029/98JA01426.

Lennartsson, O. W., L. M. Kistler, and H. Rème (2009), Cluster view of the plasma sheet boundary layer and bursty bulk flow connection, *Ann. Geophys.*, *27*, 1729–1741, doi:10.5194/angeo-27-1729-2009.

Lui, A. T. Y., L. A. Frank, K. L. Ackerson, C.-I. Meng, and S.-I. Akasofu (1978), Plasma flows and magnetic field vectors in the plasma sheet during substorms, *J. Geophys. Res.*, *83*, 3849–3858, doi:10.1029/JA083iA08p03849.

Lui, A. T. Y., T. E. Eastman, D. J. Williams, and L. A. Frank (1983), Observations of ion streaming during substorms, *J. Geophys. Res.*, *88*, 7753–7764, doi:10.1029/JA088iA10p07753.

Mason, G. M., M. I. Desai, U. Mall, A. Korth, R. Bucik, T. T. Rosengvinge, and K. D. Simunac (2009), In situ observations of CIRs on STEREO,

- Wind, and ACE during 2007–2008, *Sol. Phys.*, *256*, 393–408, doi:10.1007/s11207-009-9367-0.
- McFadden, J., C. Carlson, D. Larson, J. Bonnell, F. Mozer, V. Angelopoulos, K.-H. Glassmeier, and U. Auster (2008), The THEMIS ESA first science results and performance, *Space Sci. Rev.*, *141*, 477–508, doi:10.1007/s11214-008-9433-1.
- Mende, S. B., S. Harris, H. Frey, V. Angelopoulos, C. Russell, E. Donovan, B. Jackel, M. Greffen, and L. Peticolas (2008), The THEMIS array of ground-based observatories for the study of auroral substorms, *Space Sci. Rev.*, *141*, 357–387, doi:10.1007/s11214-008-9380-x.
- Miyashita, Y., Y. Kamide, S. Machida, K. Liou, T. Mukai, T. Saito, A. Ieda, C.-I. Meng, and G. K. Parks (2004), Difference in magnetotail variations between intense and weak substorms, *J. Geophys. Res.*, *109*, A11205, doi:10.1029/2004JA010588.
- Nakamura, M., G. Paschmann, W. Baumjohann, and N. Sckopke (1992), Ion distributions and flows in and near the plasma sheet boundary layer, *J. Geophys. Res.*, *97*, 1449–1460, doi:10.1029/91JA02361.
- Nakamura, R., W. Baumjohann, R. Schödel, M. Brittnacher, V. A. Sergeev, M. Kubyskhina, T. Mukai, and K. Liou (2001), Earthward flow bursts, auroral streamers, and small expansions, *J. Geophys. Res.*, *106*, 10,791–10,802, doi:10.1029/2000JA000306.
- Nakamura, R., et al. (2004), Spatial scale of high-speed flows in the plasma sheet observed by Cluster, *Geophys. Res. Lett.*, *31*, L09804, doi:10.1029/2004GL019558.
- Ohtani, S., and T. Mukai (2008), Statistical characteristics of the storm time plasma sheet, *J. Geophys. Res.*, *113*, A01221, doi:10.1029/2007JA012547.
- Panov, E. V., et al. (2010a), Plasma sheet thickness during a bursty bulk flow reversal, *J. Geophys. Res.*, *115*, A05213, doi:10.1029/2009JA014743.
- Panov, E. V., et al. (2010b), Multiple overshoot and rebound of a bursty bulk flow, *Geophys. Res. Lett.*, *37*, L08103, doi:10.1029/2009GL041971.
- Rong, Z. J., C. Shen, E. Lucek, A. Balogh, and L. Yao (2010), Statistical survey on the magnetic field in magnetotail current sheets: Cluster observations, *Chin. Sci. Bull.*, *55*, 2542–2547, doi:10.1007/s11434-010-3096-5.
- Sergeev, V. A., T. I. Pulkkinen, and R. J. Pellinen (1996), Coupled-mode scenario for the magnetospheric dynamics, *J. Geophys. Res.*, *101*, 13,047–13,065, doi:10.1029/95JA03192.
- Sibeck, D. G., and V. Angelopoulos (2008), THEMIS science objectives and mission phases, *Space Sci. Rev.*, *141*, 35–59, doi:10.1007/s11214-008-9393-5.
- Stone, E. C., et al. (1998), The advanced composition explorer, *Space Sci. Rev.*, *86*, 1–22, doi:10.1023/A:1005082526237.
- Sugiura, M., and D. N. Poros (1971), Hourly values of equatorial *Dst* for years 1957 to 1970, *Rep. X-645-71-278*, NASA Goddard Space Flight Cent., Greenbelt, Md.
- Takahashi, K., and E. W. Hones Jr. (1988), ISEE 1 and 2 observations of ion distributions at the plasma sheet-tail lobe boundary, *J. Geophys. Res.*, *93*, 8558–8582, doi:10.1029/JA093iA08p08558.
- Tsurutani, B. T., and W. G. Gonzalez (1995), The efficiency of viscous interaction between the solar wind and the magnetosphere during intense northward IMF events, *Geophys. Res. Lett.*, *22*, 663–666, doi:10.1029/95GL00205.
- Tsyganenko, N., and D. Stern (1996), Modeling the global magnetic field of the large-scale Birkeland current systems, *J. Geophys. Res.*, *101*, 27,187–27,198, doi:10.1029/96JA02735.
- Wang, C.-P., L. R. Lyons, V. Angelopoulos, D. Larson, J. P. McFadden, S. Frey, H.-U. Auster, and W. Magnes (2008), THEMIS observations of penetration of the plasma sheet into the ring current region during a magnetic storm, *Geophys. Res. Lett.*, *35*, L17S14, doi:10.1029/2008GL033375.
- Williams, D. J. (1981), Energetic ion beams at the edge of the plasma sheet: ISEE 1 observations plus a simple explanatory model, *J. Geophys. Res.*, *86*, 5507–5518, doi:10.1029/JA086iA07p05507.
- Zhang, T. L., W. Baumjohann, R. Nakamura, A. Balogh, and K.-H. Glassmeier (2002), A wavy twisted neutral sheet observed by CLUSTER, *Geophys. Res. Lett.*, *29*(19), 1899, doi:10.1029/2002GL015544.
- Zhang, T. L., et al. (2005), Double Star/Cluster observations of neutral sheet oscillations on 5 August 2004, *Ann. Geophys.*, *23*, 2909–2914, doi:10.5194/angeo-23-2909-2005.
- V. Angelopoulos, Institute of Geophysics and Planetary Physics, University of California, Los Angeles, CA 90065, USA.
- W. Baumjohann, R. Nakamura, E. V. Panov, A. Retinò, M. Volwerk, T. L. Zhang, and B. Zieger, Space Research Institute, Austrian Academy of Sciences, A-8042 Graz, Austria.
- A. M. Du, H. Luo, and W. Y. Xu, Institute of Geology and Geophysics, Chinese Academy of Sciences, Dwai St. Qijiahuozi, Beijing 100029, China. (amdu@mail.igcas.ac.cn)
- K.-H. Glassmeier, Institut für Geophysik und extraterrestrische Physik, Technische Universität Braunschweig, D-38106 Brunswick, Germany.
- D. Larson and J. P. McFadden, Space Science Laboratory, University of California, Berkeley, CA 94720, USA.
- Q. M. Lu, CAS Key Laboratory of Basic Plasma Physics, School of Earth and Space Sciences, University of Science and Technology of China, Hefei 230026, China.